Journal of Natural Gas Science and Engineering 40 (2017) 79–90

Contents lists available at ScienceDirect

Journal of Natural Gas Science and Engineering

journal homepage: www.elsevier.com/locate/jngse

Mechanism and application of pulse hydraulic fracturing in improving drainage of coalbed methane

Jizhao Xu [a, b, c], Cheng Zhai [a, b, c, *], Lei Qin [a, b, c]

[a] Key Laboratory of Coal Methane and Fire Control, Ministry of Education, China University of Mining and Technology, Xuzhou, Jiangsu, 221116, China
[b] State Key Laboratory of Coal Resources and Safe Mining, Xuzhou, Jiangsu, 221116, China
[c] School of Safety Engineering, China University of Mining and Technology, 221116, Xuzhou, China

ARTICLE INFO

Article history:
Received 19 May 2016
Received in revised form
31 January 2017
Accepted 1 February 2017
Available online 16 February 2017

Keywords:
Pulse hydraulic fracturing
Fatigue damage
Alternating pressure
Drainage concentration
Drainage pure volume
Permeability

ABSTRACT

Traditional hydraulic fracturing (THF) has become an effective stimulation method for the extraction of coalbed methane (CBM) and has attained many remarkable achievements in the application. However, certain problems, such as greater water pressure, larger volume of fracturing equipment, and a stricter sealing requirement, have gradually arisen in the field application. To improve the application situation, a newly developed technology of pulse hydraulic fracturing (PHF) is proposed to enhance CBM drainage via accumulating the damages in the reservoirs and weakening the rock strength by exciting oscillation from pulsating water pressure. Comparison of fracture behaviors between PHF and THF at various side-pressure ratios was executed using numerical software of PFC^{2D}; the results demonstrated that the fracture pressures required for PHF, which induced more cracks and a larger fracturing region, were all lower than those for THF. Additionally, the field application of PHF was performed for the $N_2$706 floor roadway with crossing holes in the Daxing coal mine, Liaoning Province, China. The results demonstrated that (a) all of the fracturing holes for PHF had lower fracture pressure than the calculated initiation pressure by THF, which is consistent with the simulation results; (b) the drainage parameter values of holes made via PHF, such as drainage concentration and drainage pure volume, were generally greater than those of THF. All of the simulation and application results expressed that PHF had greater superiority than THF in the application of CBM recovery based on the features of lower fracturing pressure and more cracks generation. A large amount of accumulated damage produced by PHF could greatly destroy the integrality of coal, which induced much micro-cracks generation, significantly weakening the strength of the reservoir; thus, more complicated fracture networks would be formed under a lower water pressure. Moreover, the proportion of mesopores and macropores increased after PHF, and the porosity increased by 17.29%, which indicated that PHF could significantly improve the permeability of CBM reservoirs.

1. Introduction

In recent years, the exploitation of unconventional energy, such as coalbed methane (CBM), shale gas, and renewable resources, has been a heavily researched topic in China (Su et al., 2005; Sang et al., 2010; Palmer, 2010; Cai et al., 2011; Cheng et al., 2011; Vedachalam et al., 2015; Jin et al., 2015; Chen et al., 2016). Subsequently, methods to drain these resources have been proposed, such as hydraulic fracturing, gas injection displacement, and other techniques (Huang et al., 2014a,b; Wang et al., 2014a; Ferrer and Thurman, 2015; Li et al., 2016). In China, CBM reservoirs commonly have low permeability and a dense coal matrix (Sang et al., 2010; Liu et al., 2011; Wang et al., 2014a; Jin et al., 2015). Hydraulic fracturing is an effective technical approach to resolve the challenges of gas extraction from low-permeability coal seams (Huang et al., 2011, 2012; Shimizu et al., 2011; Zhang, 2014; Cheng et al., 2015). This technology can alter the structure of the coal mass by increasing the number and density of cracks in the mass to improve permeability. Many studies on hydraulic fracturing have been conducted both in China and in other countries during the past few decades (Huang et al., 2011; Zhang, 2014; Zhao et al., 2014;

* Corresponding author. Key Laboratory of Coal Methane and Fire Control, Ministry of Education, China University of Mining and Technology, Xuzhou, Jiangsu, 221116, China.
E-mail address: greatzc@126.com (C. Zhai).

http://dx.doi.org/10.1016/j.jngse.2017.02.012
1875-5100/

Yoon et al., 2015; Zhou et al., 2014). Several field investigations (Nakao et al., 2000; Zhou et al., 2010; Sesetty and Ghassemi, 2015; Wang et al., 2015) have indicated that traditional hydraulic fracturing (THF) techniques fracture rocks using a constant water pressure that is greater than the rock strength. In general, THF requires high flow, high pressure and large amounts of water; devices providing these features may be difficult to acquire. For example, high flow requires large-volume equipment, which is not suitable for narrow roadways in underground coal mines; high pressure necessitates more complicated sealing technology and markedly increases hidden dangers (Zhai et al., 2011, 2012, 2015a; Lu et al., 2014, 2015), which both fails to satisfy the production requirement and results in some seismic hazards.

To improve the existing deficiencies of THF and to produce complicated fracture networks, pulse hydraulic fracturing (PHF) was proposed, which combines the advantages of THF and a variable-frequency pulsating load (Vijay et al., 1993; Zhao, 2008; Li et al., 2011; Lu et al., 2014, 2015). The foremost distinction between THF and PHF is the mechanism of fracturing coal; specifically, the THF process uses only high water pressure and the injection pressure is related to the original ground pressure. In contrast, PHF incorporates the mechanism of fatigue damage based on the function of THF. Specifically, this technique involves the injection of pulsating water at variable frequencies into the fracturing borehole. Persistent pulsating waves spread into the interior of the coal rock mass and periodic alternating stress, generated by the peak pressure and the bottom pressure, exerts repeating loads on the coal mass. Finally, fatigue damage of the internal coal mass gradually becomes apparent from the effect of cyclic loading with different frequencies. Many studies (Liang et al., 2012; Liu and He, 2012; Zhu et al., 2013, 2014; Hu et al., 2016) have proposed that the cyclic loading could increase internal fatigue damage and decrease the rock strength with different loading rates to varying degrees. Finally, PFH could easily fracture a fatigued coal mass with a lower injection water pressure.

A coal mass contains numerous flaws, from bedding-scale to pore-scale, making the coal mass anisotropic. Compared with the fracturing process under uniaxial compression, which relies on external force to break down rocks, from the macroscopic viewpoint, the fracturing behavior of PHF in the coal seam is in virtue of the ‘extrusion-splitting’ effect of water to the walls of the flaws, which causes the flaws to open into cracks and enhances the extension of cracks. At the micro-level, pulsating water possesses two action mechanisms: one is that the high frequency stimulates the removal of pore blockages by fatigue fracturing, thus opening the gas-flow path and improving the circumjacent permeability; the other is that the pulsations decrease the strength of the coal rock to less than the maximum value from constant pressure loading (Zhai et al., 2011; Wang et al., 2015).

Micro-fractures are nucleated by fatigue damage and begin to extend constantly as a result of continued cyclic loading. This process connects natural cracks, joints, and bedding, and the cracks continue to propagate and evolve into a complicated fracture network (Lu et al., 2014, 2015). Dehkhoda and Hood (2013) investigated the relative contributions of pulse length and pulsation frequency on the surface and sub-surface damage caused by a pulsed water-jet on rock targets. Previous studies demonstrated that the magnitude of failure zones was related to the pulsation frequency, and the sub-critical cracks, which propagated to cause major rock-failure, depended on the pulse length. To improve the gas drainage of high-gas, low-permeability coal seams, hydraulic fracturing experiments and mechanical analysis were conducted under different pressures and frequencies and the fatigue characteristics of coal and the mechanism of PHF were analyzed by Zhai et al. (2011). Lu et al. (2014, 2015) presented a numerical stress-disturbance model to simulate the formation stress response during PHF, and the concept of the effective stress disturbance zone was proposed. The variations of PHF effects under different coal seam conditions (Young's modulus, Poisson's ratio, and horizontal *in situ* stress) and the influences of the technical parameters (frequency, amplitude, and mean stress) on the PHF stress disturbance effect were investigated. Li et al. (2013a,b) investigated fracture modes with variable frequencies and a single frequency using a pressure sensor and acoustic emission (AE) and concluded that the effect of variable frequency on fracture extension is more pronounced than that of single frequency. Additionally, different combinations of frequency and pressure were investigated for proposed dual frequency-dual pressure fracturing technology. Li et al. (2013) used a theoretical review, laboratory experiments, and field tests to investigate the generation and propagation of the pulsating stress wave and the breakage mechanism, moreover, the difference between THF and PHF was investigated through laboratory tests. Zhai et al. (2015a) studied relationships describing pulsating water pressure (PWP) propagation during PHF in a two-dimensional fissure simulator at different pulse frequencies and plugging rates and described the relationship between PWP peak pressure and the plugging ratios. Ni et al. (2014) experimentally studied the kinetic characteristics of gas desorption in terms of pulsating injection (PI) and hydrostatic injection (HI). That study indicated that the initial velocity, diffusion capacity, and ultimate amount of methane desorption after PI are greater than those after HI and that the methane decay rate over time is less than that of HI. Li et al. (2015) carried out on-site application of PHF in the Yuwu coal mine, China, and demonstrated the promise of this application in the future prevention and control of coal and gas outburst hazards.

To characterize the features of PHF preferably and verify the fracturing effect in the field application objectively, this study is composed of three main parts, including an introduction to PHF, numerical stimulation using the software Particle Flow Code 2D (PFC^{2D}, Itasca software) and field application. First, the fundamental principal, main equipment attachment and sealing technology of PHF is introduced; second, the numerical stimulation ias executed to characterize the differences of fracturing pressure and fracture morphology, comparing PFH with THF; finally, the field application of PHF is located in the $N_2$706 floor roadway with crossing holes to the coal seam, Daxing coal mine, Liaoning Province, China, and the effect of PHF is determined based on two aspects: gas drainage parameters and permeability change. All of the simulation results and application results are conducive to popularizing the PHF technique for CBM effective extraction in the future.

2. Introduction of PHF

2.1. Fundamental principle of PHF

During the PHF process, the pulsations of pressured water with different frequencies exert a load on the wall of the boreholes, preferentially causing fatigue damage relative to the single fracturing method. Eventually, cumulative fatigue damage is caused by the cyclic loading–unloading–loading pattern, which decreases the elasticity modulus and the strength of the coal seam. Thus, PHF fractures coal effectively via the coupled effects of pressure and fatigue.

After drilling, the original stresses redistribute around the holes, and four regions, i.e., fracture zone, plastic zone, elastic zone, and primary rock stress zone, can be delineated based on the different conditions at various distances from the fracturing hole. Water fills in the fracturing hole, flowing into the fracture zone along the abundant cracks. To describe the propagation of pulse water pressure in fractures, three models are relevant: the flow model in porous media, the water turbulence model, and the transient flow model (Li and Liu, 2005). Based on the one-dimensional compressible unsteady equation, Fiorotto and Rinaldo (1992) established the one-dimensional transient flow model:

$$\begin{cases} \frac{\partial p}{\partial t} + u\frac{\partial p}{\partial x} + \frac{c^2}{g}\frac{\partial u}{\partial x} = 0 \\ \frac{\partial u}{\partial t} + u\frac{\partial u}{\partial x} + g\frac{\partial p}{\partial x} + \frac{\psi}{4\zeta}|u|u = 0 \end{cases} \tag{1}$$

where p is the waterhead, x is the direction of the fracture path, t is the flow time, u is the velocity of water flow in the fracture, c is the characteristic wave velocity, g is gravitational acceleration, ζ is the width of the aperture, and ψ is the obstruction coefficient, which is related to the roughness of the aperture.

Based on the propagation rule of pulse pressure from water in fractures in the transient flow model, Professor Liu (1994, 1998) considered that the pulse pressure in fractures transiently propagates into the internal rock as an approximately constant wave. In contrast, PHF generates pulse pressure water, which propagates as waves in fractures (Li, 2013). When a fracture is not penetrated, the pulse water readily generates eddies, in which larger eddies contain small eddies and small eddies contain smaller eddies. Meanwhile, because of the effect of the water boundary, i.e., the fracture plane, the pressure wave has two mechanisms: one is propagation into the rock interior, inducing rock shock; the other is reflexing and superposition, producing a transient phenomenon similar to a water hammer. This coupled mechanism is characteristic of PHF and is more effective in producing cracks than THF.

For PHF, the water pressure could be defined by the sine function (Li, 2013): $P = A\sin\left[\omega\left(t - x/_{c}\right) + \varphi\right]$, where A, ω, φ, x, and c represent the amplitude, angular velocity, initial phase, distance to the pump body, and wave velocity, respectively. Propagation of the pulse pressure wave into the rock interior stimulates grain vibration along random directions. Long-term vibrations alter the connections between grains, weakening the strength of the connection in several ways. The weakening process causes the rock to experience fatigue; finally, plastic yield occurs. Using the continuum damage mechanics of elastic plastic materials from Xie et al. (1997), the amount of damage can be calculated by:

$$D = 1 - \frac{\tilde{E}}{E_0}\frac{\varepsilon_0 - \tilde{\varepsilon}}{\varepsilon_0} \tag{2}$$

Where $\tilde{\varepsilon}$ and ε_0 are the strain after and before stress, respectively, and $\tilde{E}$ and E_0 are the elasticity modulus after and before stress, respectively.

Thus, after injecting time t of pulse pressure from PHF, the strength of the affected rock is reduced according to the periodicity of the sine function:

$$\tilde{\sigma} = \sigma_0\left(\frac{\varepsilon_0 - \tilde{\varepsilon}}{\varepsilon_0}\frac{\tilde{E}}{E_0}\right)^{\frac{2\pi t}{\omega}} \tag{3}$$

Accordingly, the critical stress value for the destruction of rock after PHF is:

$$\tilde{\sigma}_c = \sqrt{\frac{2\tilde{E}\gamma}{\pi C}} \tag{4}$$

where C is crack length, γ is surface energy.

Because the critical stress value and the strength of rock gradually reduce as the duration of pulse injection increases, only if the peak stress of the pulse pressure exceeds $\tilde{\sigma}_t$ (the tensile strength, consistent with Eq. (3) in form) will cracks be generated in materials. When the breaking strength in the crack tip is more than $\tilde{\sigma}_c$, the crack will propagate until the material fails entirely.

2.2. Main equipment attachment

Before fracturing, devices such as the water tank, pulse injection pump, frequency converter, overflow valve, and other valves were connected in turn, as illustrated in Fig. 1. A pulse pump with a maximum pressure of 25 *MPa* and a mass flow of 130 *L*/min was used as the power equipment. A frequency converter with an adjustable frequency range of 0–25 *Hz* and an overflow valve were used as controlling equipment. Relevant safety checks were carried out successively, e.g., whether the tube coupling was right, whether the *U*–type clips were deficient, and whether anybody was in the warning lines.

2.3. Sealing technology

To seal the fracturing holes, we combined the advantages of expansive cement and packers. This sealing method provides high compression strength and guarantees that the fracturing holes can be repeatedly used to drain CBM and for fracturing. Following the method of Li et al. (2015), the systematical PHF sealing method first involved placement of a Polyvinylchloride (PVC) tube into the fracturing hole; both ends of the PVC tube were blocked to form a grouting space, which was filled with expansive cement. Subsequently, a packer that was injected with water or air at pressure P_{pacp} and was passed through by the fracturing pipe was put into the PVC tube. Next, the injected pressure in the packer was released and the packer was removed after PHF. To seal the drainage holes, we used flexible gel, which was injected in the grouting space between the PVC tube and the wall of the hole (Zhai et al., 2015b). Finally, all the PVC tubes were connected to the gas drainage network and CBM was extracted via negative pressure.

3. Numerical simulation of PHF

Coal rocks are heterogeneous materials comprising cemented complex-shaped grains at the micro- and macro-scale; the anisotropic nature can be observed with the naked eye readily (Cho et al., 2007). The bonded-particle model for rock could directly mimic the fidelity of a rock system and then exhibits a large set of emergent behaviors, which correspond well to those of real rock (Potyondy and Cundall, 2004). The Particle Flow Code (PFC), developed by the ITASCA Consulting Group, models a rock mass as an assemblage of non-uniform-sized circular or spherical particles that are bonded together with soft contact and that possess finite normal and shear stiffness. Here, it is noted that the term ‘particle’ is taken as a body of negligible size that occupies a finite amount of space. The mechanical behaviors are described by the movement of each particle and the force exists at each contact (Potyondy and Cundall, 2004). There are two bond models among particles: contact bond model and parallel bond model, in which the former only transmits force at an infinitesimal contact point, while the latter delivers force and moment at a finite circular section. These bonds will break when the applied local stresses exceed the specified bond strength. For the contact bond model, the breaking of bonds will not influence the macro stiffness if the particles reserve to contact. For the parallel bond model, the breaking of bonds will result in the decrease of macro stiffness, which is suitable for stimulating the coal rock (Wang et al., 2014b). Thus, the parallel bond model is used to compare the crack behaviors of PHF and THF.

A ‘domain’ is defined as a closed chain of particles such that each

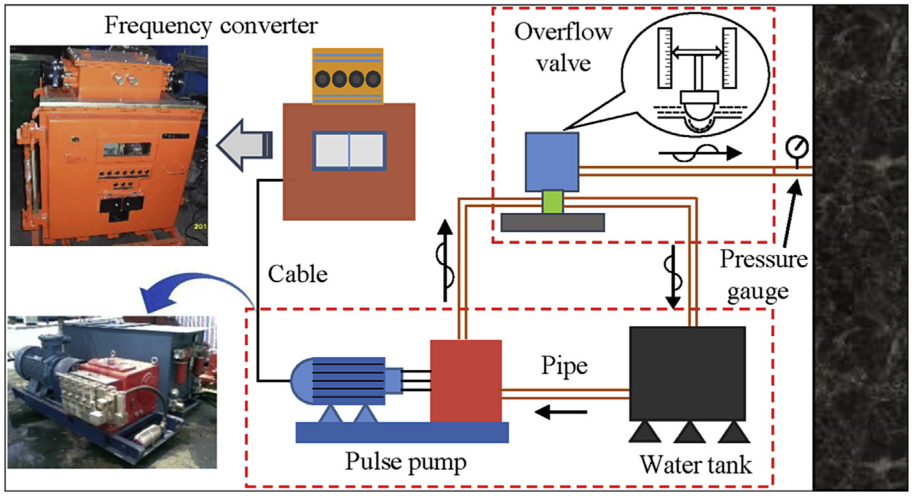

Fig. 1. Configuration of the PHF setup in the field.

link in the chain is a parallel bond, as shown in Fig. 2. Meanwhile, each link, termed a 'pipe', between two adjacent domains is a potential crack. The 'pipe' is both a flow path for fluid and a channel connecting other domains. The aperture of the crack is in direct proportion to the normal displacement of the parallel contact. As far as the fluid is concerned, the water pressure is applied to each particle as a body force in the 'domains'. A 'pipe' is equivalent to a parallel-plate channel, with length (L), aperture (a), and unit depth; thus, the flow rate in a pipe is given by:

$$q = \frac{a^3}{12\mu}\frac{P_2 - P_1}{L} \tag{5}$$

where μ is the fluid viscosity of water and $(P_2 - P_1)$ is the pressure difference between two adjacent domains.

Each domain experiences water pressure acting on the free surfaces of the particles from the surrounding pipes: $\sum q$. Assuming that the inflow is positive, the increase in fluid pressure once step, Δt, is:

$$\Delta P = \frac{K_f}{V_d}\left(\sum q\Delta t - \Delta V_d\right) \tag{6}$$

where K_f is the water bulk modulus and V_d is the apparent volume of the domain.

Considering a pressure perturbation, focusing on all the pipes and applying pressure to all the domains, the flow into the domain can be calculated by solving the following equation:

$$Q = \frac{Ma^3K_f q\Delta t}{24\mu RV_d} \tag{7}$$

where M is the number of pipes connected to the domain and R is the mean radius of the particles surrounding the domain.

Based on the above fluid–solid coupling mechanism in PFC^{2D}, we established three groups of samples with a length and width of 20 *m*, the porosity of which is 0.15; the number of particles in the model is 2703. Additionally, the particular parameters of the model design are shown in Table 1. Before exerting the side pressure, the particle assemblage was in an equilibrium state. Different side pressure ratios k (>1, $=1$, and <1) were used to simulate the primary stress via servo-control, as shown in Fig. 3 (a). Additionally, a fracturing hole with a radius of 0.1 m was drilled in the center of the sample. The initial pore pressure was set at the beginning of calculation; hence, water was injected with a constant pressure for THF, while with a periodic variation pressure of water for THF. The finishing criterion of fracturing was when cracks or fractures propagated to the border of the sample within a certain time.

Fig. 3 (b) shows the crack propagation and the water flow paths after PHF and THF for different side pressure ratios k. The red line segments and various sizes of deep-red circles indicate the induced cracks and flow pressure, respectively. If the water stress difference between adjacent domains exceeds the bond, then the 'pipe' breaks and a crack is generated. The flow paths were along the fracture propagation direction, which confirms the law that cracks are always along the direction perpendicular to the minimum principal stress. For example, for $k > 1$, the transversal stress σ_1 was greater than the vertical stress σ_2, and the crack propagation direction and flow path were generally along the direction of σ_1. Additionally, the fracture pressure of PHF was less than that of THF for each same side pressure ratio. All the samples of PHF had a larger area than those of THF, and at $k = 1$, the THF flows could not fracture the sample and only produced some fractures around the hole; in contrast, PHF produced a complicated fracture distribution and larger fracture region.

Fig. 4 shows that the number of accumulated cracks increased persistently and showed various increments during PHF and THF, with different values of k until the fracturing process had finished. As the time step increased, the final crack numbers of the specimen

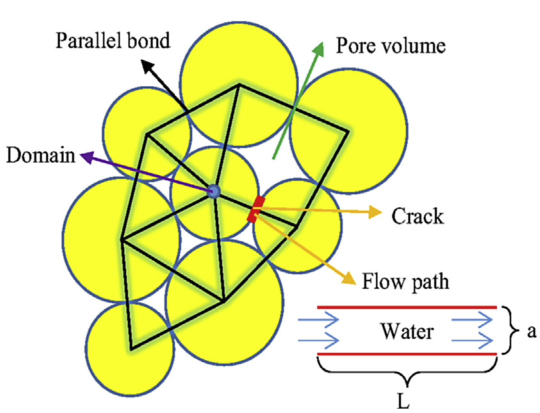

Fig. 2. Domains and flow path in a parallel-bonded assembly of particles.

Table 1
The mesoscopic parameters of the PFC model.

Particle basic parameters		Parallel bond parameters	
Particle density ρ (kg/m^3)	2000	Mean shear strength $\overline{\tau}$ (MPa)	9
Minimum radii $r_{\min}$ (m)	0.15	Standard deviation of shear strength $\overline{\tau_s}$ (MPa)	0.1
Size ratio $r_{\max}/r_{\min}$	1.6	Mean normal strength $\overline{\sigma}$ (MPa)	9
Contact modulus E (GPa)	0.8	Standard deviation of normal strength $\overline{\sigma_s}$ (MPa)	0.1
Stiffness ratio k_n/k_s	1	Elastic modulus $\overline{E_c}$ (GPa)	0.8
Friction coefficient μ	0.3	Stiffness ratio $\overline{k_n}/\overline{k_s}$	1
Damping constant γ	0.7		

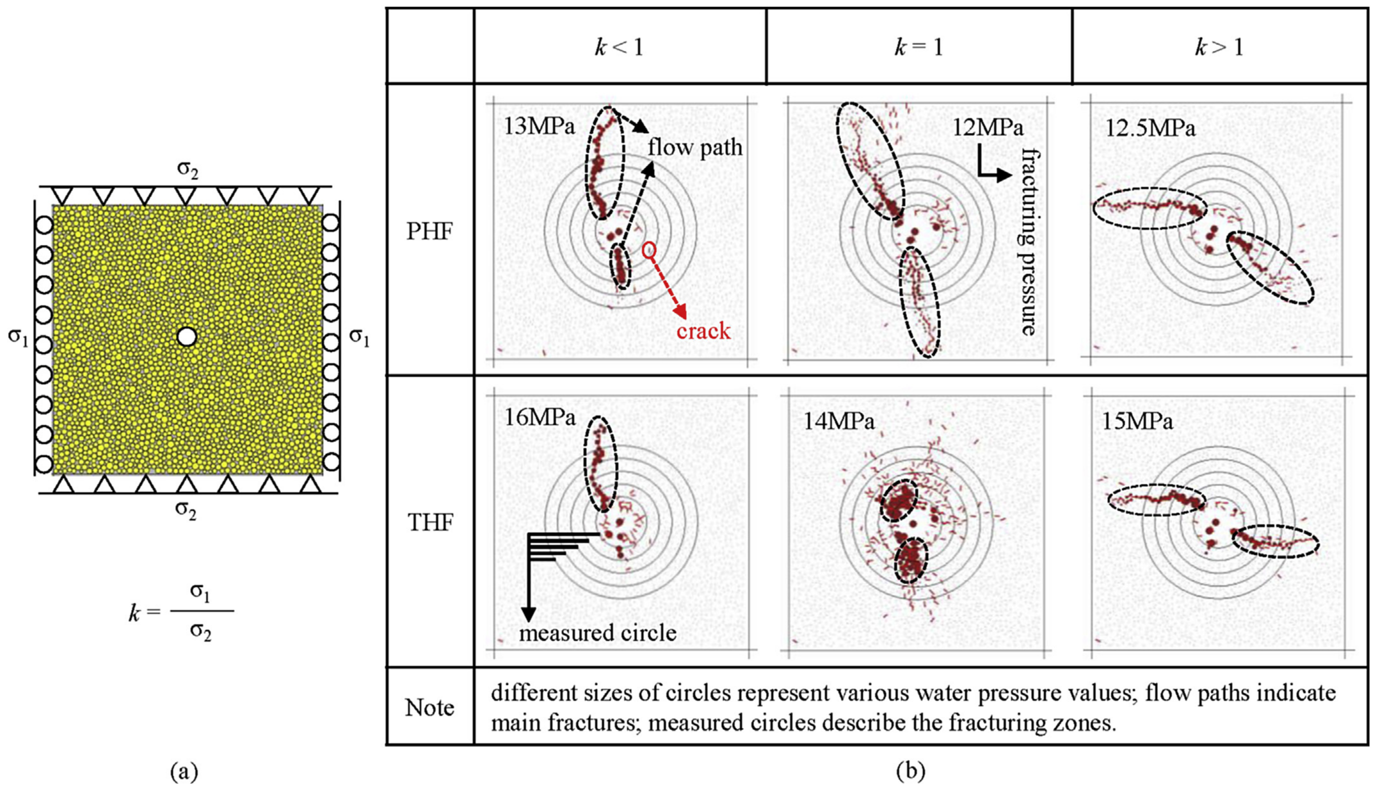

Fig. 3. Numerical simulation of PHF and THF for $k < 1$, $k = 1$, and $k > 1$: (a) the final sample model at different side pressures σ_1 and σ_2; (b) results of fracturing by PHF and THF for $k < 1$, $k = 1$, and $k > 1$, showing cracks, flow paths, and crack regions.

at $k < 1$ or $k > 1$ for PHF were greater than those for THF, assuming that the final numbers of cracks from PHF at $k < 1$ and $k > 1$ were 14 and 9 more than those from THF, respectively. Although the results of crack numbers were almost the same at $k = 1$ for both PHF and THF, the cracked region for PHF was broader than for THF, as illustrated in Fig. 3. Moreover, the incremental number of cracks in PHF showed a larger difference from step 4×10^5 to the final step, which might be related to the appearance of internal fatigue damage and the decrease in strength. Thus, the fracturing effect from PHF was better than that from THF.

4. Field application

4.1. General engineering situation

The Daxing coal mine is located in the southwest part of the Tiefa Coalfield in Liaoning Province, China, as shown in Fig. 5. The working face of $N_2$706 is located in the middle of the north second panel; it has a length, width, and area of 348–513 m, 165–180 m, and 147 285 m^2, respectively. According to the gas-geological map, this working face possesses a high concentration of CBM, i.e., 2.79–21.05 m^3/t, with a mean value of 8.03 m^3/t. The pressure of CBM is 0.35–0.79 MPa and the permeability is low. To improve mining safety, the CBM should be pre-extracted to reduce the danger of a gas outburst. After considering many factors, such as the complicated stratigraphic texture and the layout pattern of roadways, *i.e.*, the 706 working face and the floor roadway, we selected the crossing boreholes from the $N_2$706 floor roadway to the coal seam as the study area.

4.2. Project design of PHF with crossing boreholes

We tested the PHF process with crossing boreholes. Specifically, we drilled fracturing holes and extraction holes in the floor roadway, finally terminating at the 7th coal seam. We used PHF to fracture the 7th coal seam and improve its permeability, with the goals of effective extraction and mining safety.

The fracturing holes were arranged in the soft walls of the $N_2$706 floor roadway. There was a total of six holes, placed where there was an abandoned hole. The dip angles of all fracturing holes were

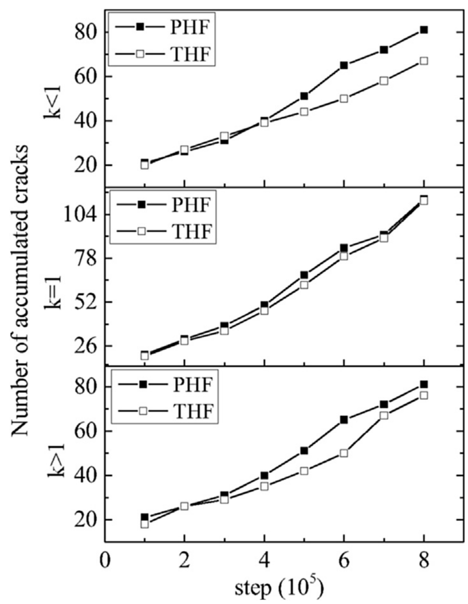

Fig. 4. Number of accumulated cracks through time for $k < 1$, $k = 1$, and $k > 1$.

consistent within 20°. The guide holes were drilled along the directional fracturing path and were placed 5–6 m away from both sides of the fracturing holes. All these guide holes were also used as drainage holes to extract CBM. The dip angle of guide holes was 20 ± 3°. All the holes terminated at the 7th coal seam and the drilling process was finished prior to the commencement of fracturing. The parameters of the fracturing holes and extraction holes are listed in Table 2. The spatial layout of holes is shown in Fig. 6.

4.3. Selection of PHF parameter values

The coal seam is subject to triaxial stress caused by the overlying rock and possesses a certain degree of strength from long-term compression. According to the analysis of forces around a fracturing hole and classical fracturing theory (Hubbert and Willis, 1957), the initiation fracture pressure is influenced by many factors, such as *in situ* stress and rock strength (Li et al., 2015); thus, the initiation fracture pressure could be calculated by:

$$P_{ini} = \sigma_t + 3\overline{\sigma}_3 - \overline{\sigma}_1 \tag{8}$$

where σ_t is the tension strength of the coal seam (MPa); $\overline{\sigma}_1$ and $\overline{\sigma}_3$ are the maximum and minimum effective principal stress, respectively (MPa); $\overline{\sigma}_i = \sigma_i - \zeta P_{pore}, (i = 1, 3)$. σ_i and P_{pore} are the principal stress and pore stress, respectively; and ζ is the pore pressure coefficient.

Based on the ground stress measurement results from using hollow inclusion cells (Kang and Feng, 2012) and after calculating the difference between the stress of overlying rock and the effective vertical principal stress, the pore pressure, maximum principal stress, and minimum principal stress are 1.34, 28.4, and 20.27 MPa, respectively. The tensile strength of coal is 2.31 MPa, and ζ is set to 0.8. Thus, the value of P_{ini} is 30.27 MPa. From this, the initiation fracture pressure of THF is set at 30.27 MPa.

From the pre-test results of PHF physical experiments, the injecting frequency was set from 6 Hz to 24 Hz. According to the sealing theory and process of PHF from section 2.3, the required packer pressure P_{pacp} in the upward-crossing holes from the 706 floor roadway to the 7–2 coal mine must be calculated first. A mechanical model for an expanding packer under fracture water pressure loads was estimated, as shown in Fig. 7.

To guarantee the packer in the PVC tube would not being rushed out, the force condition meets the following equality:

$$\begin{cases} F_{fric} = \lambda(P_{pacp}S_{pac} + mg\cos\theta) \\ F_{peak} = P_{iwp}S_{pvc} + mg\sin\theta \\ F_{fric} \geq F_{peak} \end{cases} \tag{9}$$

where F_{fric}, is the frictional force between the packer and the PVC tube; F_{peak} is the peak pressure from the pulse water pressure and packer self-gravity. P_{pacp} and P_{iwp} are the pressure of the expanded packer and the peak pressure pulse water (MPa); S_{pac} is the circumferential contact area between packer and PVC tube, (m^2); and S_{pvc} is the cross-sectional area of the PVC tube, (m^2); λ is the friction coefficient between the packer and the PVC tube; m is the weight of the expanded packer; and θ is the angle between the fracturing hole and the horizontal plane.

From this, the required packer pressure P_{pacp} could be calculated as follows:

$$P_{pacp} \geq \frac{1}{S_{pac}}\left[\frac{1}{\lambda}(P_{iwp}S_{pvc} + mg\sin\theta) - mg\cos\theta\right] \tag{10}$$

According to Eq. (8), the maximum initiation pressure of this working face is 30.27 MPa, so P_{iwp} should be 30.27 MPa. Based on test results for the packer, m is 30.144 kg (for two packers) after expanding and filling with water. S_{pac} and S_{pvc} are 1.5072 and 0.0113 m^2, λ is 0.5, and θ is 20°. Thus, P_{pacp} is 0.45 MPa, and in this study, P_{pacp} is set to 0.45 MPa.

5. Results and discussion

5.1. Results of PHF

After a period of PHF, running water appeared at all the guide holes. This was regarded as the end of the fracture process, and the fracture holes and guide holes were connected to the CBM drainage network. Detailed information on all the fracturing holes is provided in Table 3. Scatterplots of the main parameters of all fracture results and a comparison of the pressure between PHF and THF are shown in Figs. 8 and 9.

From Fig. 8, there exists a positive correlation between duration and water volume (fitting coefficient 0.9643), as well as fracturing radius (fitting coefficient 0.966), i.e., the longer the duration, the greater the water volume and the greater the fracturing radius. However, fracturing radius seems to increase slowly as duration increases, which might be influenced by the geologic structures. The initiation pressures for PHF were 25.7, 22.4, 26.7, 23.9, and 27 MPa and the calculated initiation pressure was 30.27 MPa, as shown in Fig. 9, in good agreement with the results of the theoretical calculation, as described in Section 2. Additionally, the fatigue effect of PHF decreased the initiation pressure by 10.8%–26%.

5.2. Variations in gas drainage data

After all the fracturing holes and guide holes had been connected to the drainage network, we used a gas gauge to measure the drainage concentration and drainage pure volume three times a day. Data logging persisted for almost 2 months. Three groups of drainage data were averaged daily: the monitored gas drainage data, fracturing holes #1, #3, and #5, and guide holes #1–2, and #3–4 were selected to be the observation subjects to determine the variation in their drainage parameters. Fig. 10 shows the variation of the drainage parameters of these five selected holes.

During monitoring over a period of 60 days, all the fracturing

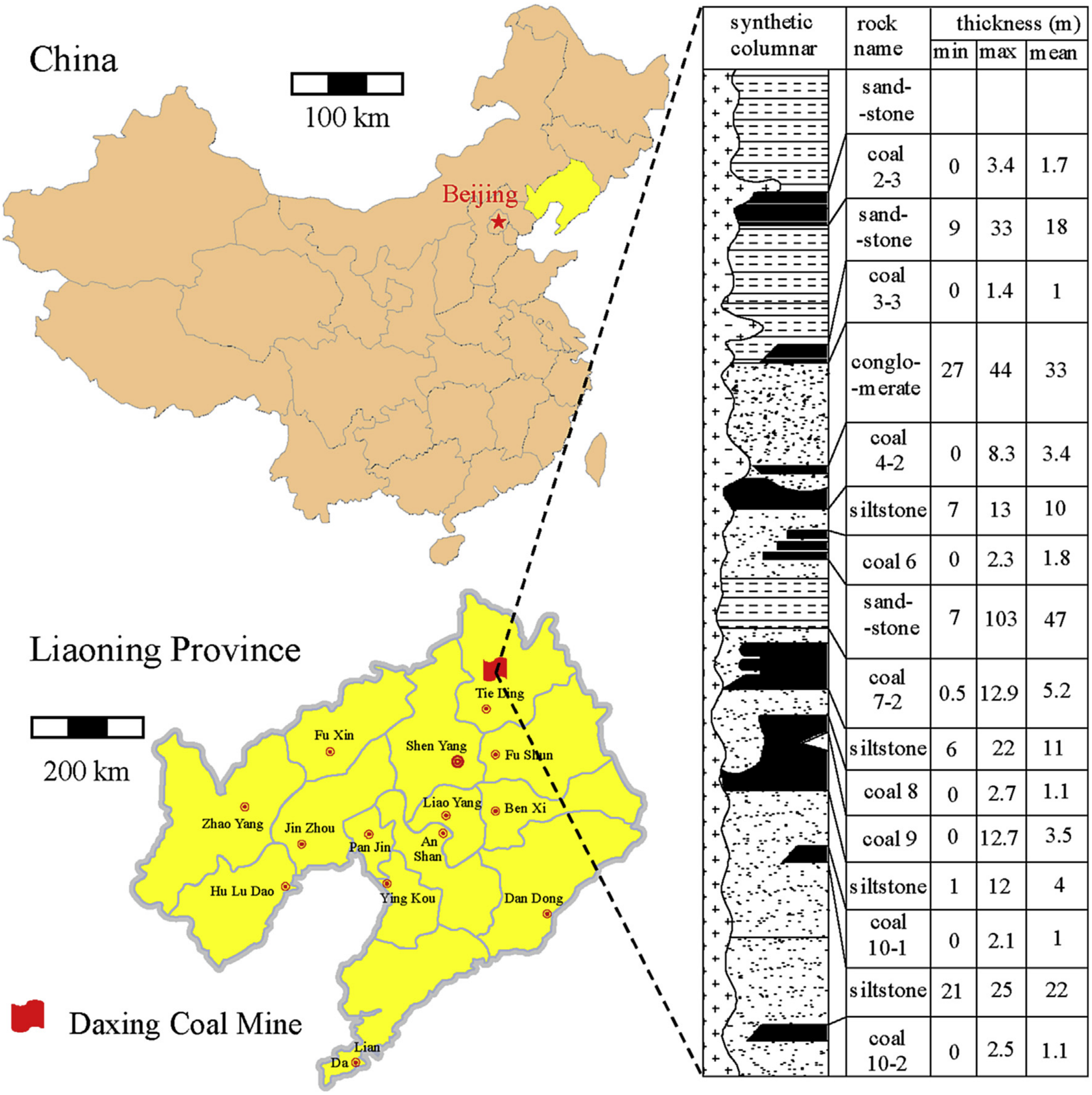

Fig. 5. Geological map of Daxing coal mine, Liaoning Province.

Table 2
Parameters of fracturing holes and extraction holes.

Location	Hole type	Diameter (mm)	Hole depth (m)	Dip angle (°)	Horizontal angle (°)
N2706 floor roadway	fracturing	133	35–60	20	90
	guide (drainage)	133	35–60	20 ± 3	90

holes and guide holes showed approximately similar variation of drainage parameters, including drainage concentration and drainage pure volume. The variation displayed a decreasing–increasing–decreasing pattern in all the curves. Based on this pattern, the process was divided into three phases: water blocking, rising, and attenuation. During the initial drainage process, many cracks were generated after PHF and large amounts of CBM were expelled. With the effect of water blocking (Ni et al., 2016), the drainage parameters of CBM began to decrease. As the water evaporated under the effect of negative air pressure in the drainage network, the propagated cracks provided many flow paths for CBM drainage. The maximum drainage concentration and drainage pure volume were 45% and 0.43 m^3/min, respectively. Moreover, the drainage parameters of fracturing holes were more than those of the guide holes during the attenuation phase, which indicated that the greater the number of cracks, the larger the apertures of cracks generated around fracturing holes, whereas there were fewer cracks with smaller apertures around guide holes; thus, for the same desorption and drainage negative pressure, the attenuation velocity of fracturing holes was less than that of guide holes.

To compare the fracturing effect of PHF with that of crossing holes and THF, we selected some THF holes, i.e., the # 3 hole of group 23, # 4 hole of group 24, and # 4 hole of group 30, in the same floor roadway. Fig. 11 shows the difference in drainage parameters between the PHF holes (# 2, # 4, # 5) and the three groups of THF holes during a 2-month period. For drainage concentration, on day

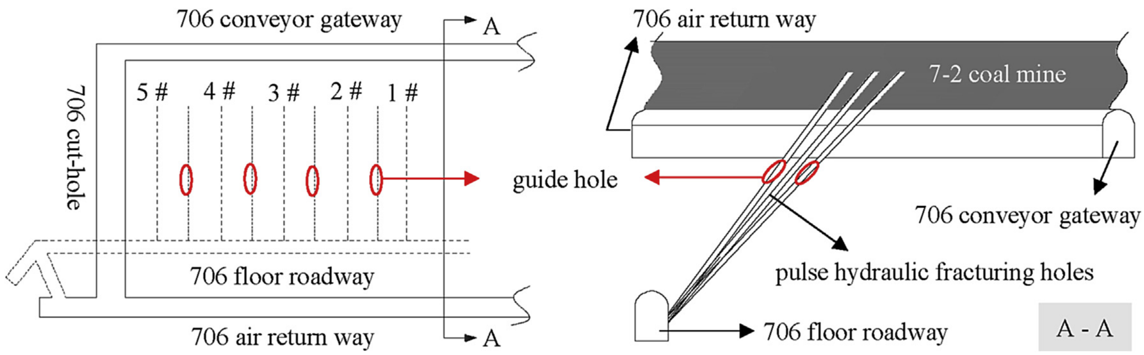

Fig. 6. Layout of crossing pulse hydraulic fracturing holes and guide holes in the design phase and site operation.

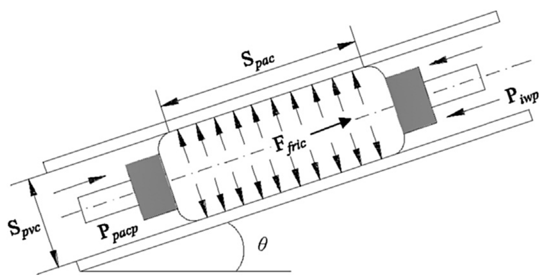

Fig. 7. Mechanical model of an packer in a fracturing hole.

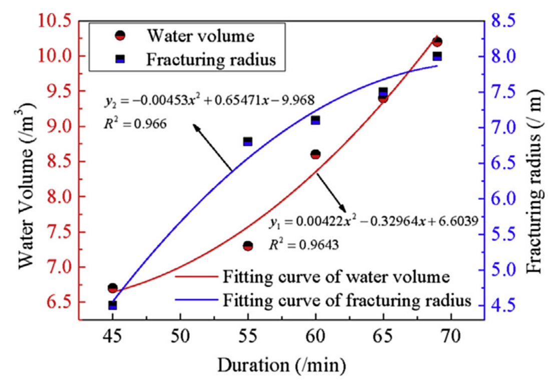

Fig. 8. Main parameters of all the PHF fracturing holes.

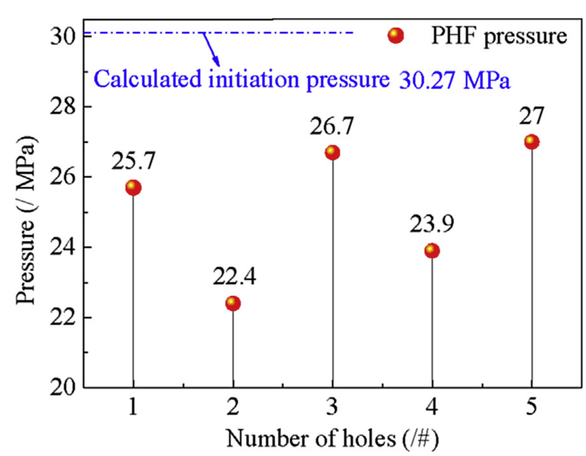

Fig. 9. Values of PHF pressure and initiation THF pressure.

28, the value for PHF was 38%–42%, while that for THF was 22%–29%; on day 60, the values for PHF and THF were 25%–32% and 12%–13%, respectively. Thus, from the comparison of concentration variation, PHF had more dominance and effect in drainage concentration than THF. Furthermore, the drainage concentrations from PHF exhibited some fluctuations, which might be related to internal micro-cracks generated by the PHF fatigue loads. These micro-cracks provided persistent flow paths for CBM migration, whereas the concentration from THF solely decreased without induced micro-damage. Meanwhile, in terms of drainage pure volume, a change was apparent on day 13. The pure volume of PHF increased then decreased; that of THF persistently decreased. On the final day, the pure volume of PHF was 0.2–0.27 m^3/min and the value for THF was 0.05–0.1 m^3/min. To simplify the quantification analysis, the two-dimensional area was used to calculate the difference between the two fracturing methods.

Fig. 11 represents the gap with two areas S_c and S_{pv}, and the areas were calculated by

$$S_c = \frac{(c_1 + c_4 - c_2 - c_5)(t_3 - t_1)}{2} - \frac{(c_1 - c_4)(t_3 - t_2)}{2} \tag{11}$$

where t_1, t_2, and t_3 are the various day when obvious difference occurred, and c_1, c_2, c_3, c_4, and c_5 are concentration values on relevant day respectively.

Table 3
Details of all the PHF fracturing holes.

	Sealing length/m	Duration/min	Water volume/m^3	Fracturing radius/m	Frequency/Hz	Pressure/MPa	Sealing effect during PHF
# 1	21	69	10.2	8	10–24	25.7	well
# 2	19	65	9.4	7.5	15–25	22.4	well
# 3	22	55	7.3	6.8	10–20	26.7	well
# 4	20	45	6.7	4.5	8–20	23.9	well
# 5	18	60	8.6	7.1	12–22	27	well

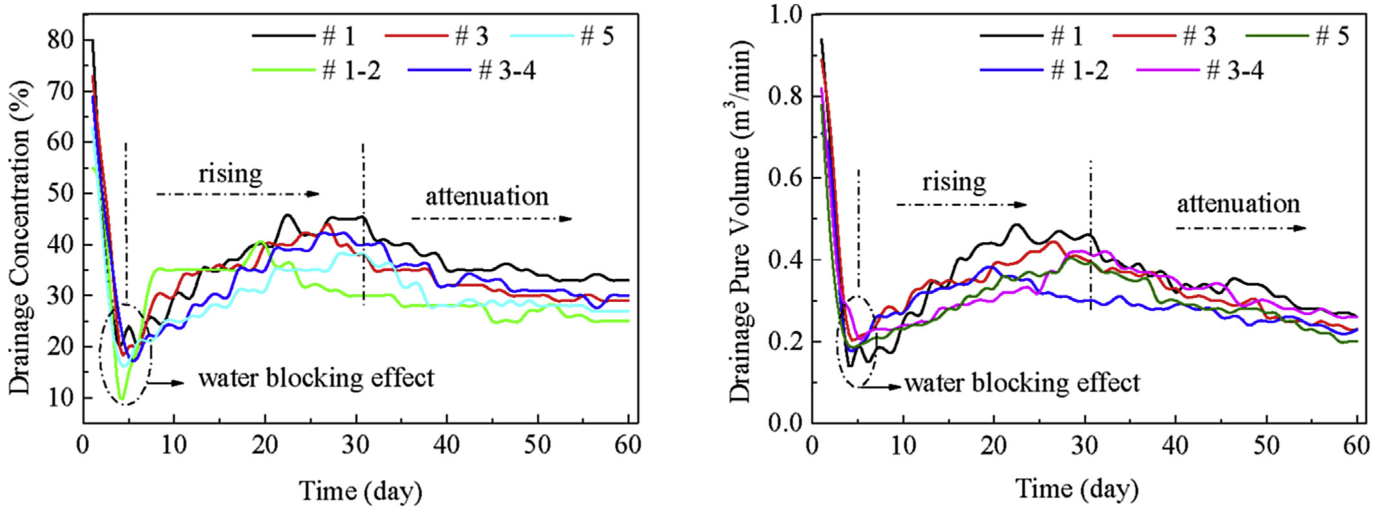

Fig. 10. Variation of drainage parameters of fracturing holes # 1, # 3, and # 5 and guide holes # 1–2 and # 3–4 during a 60-day period.

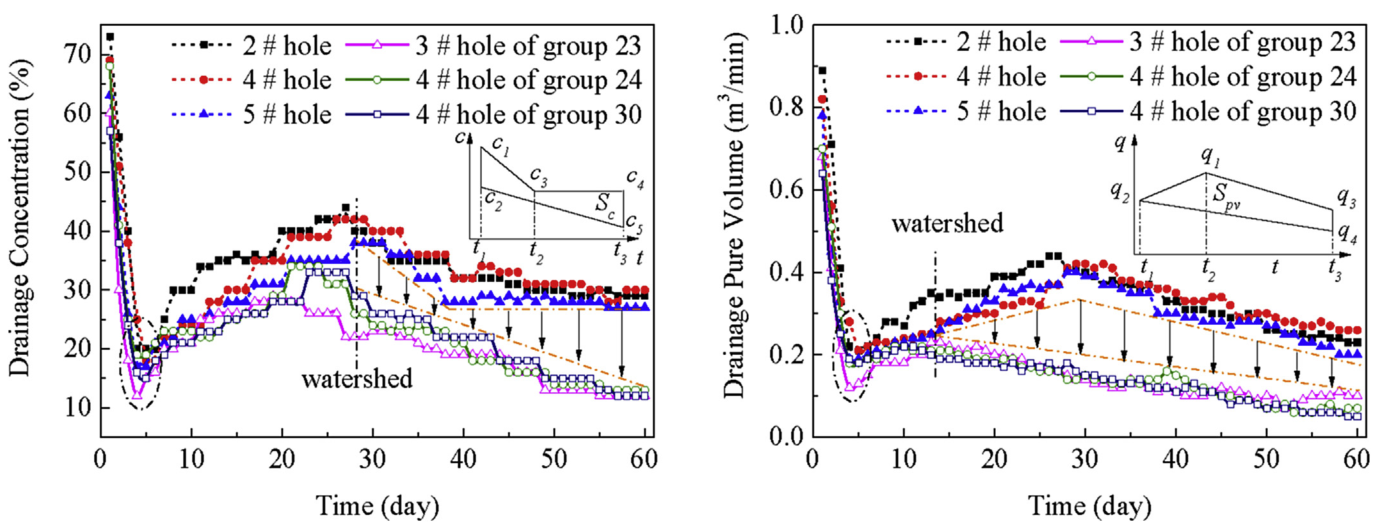

Fig. 11. Difference in drainage parameters between PHF holes (2 #, 4 #, and 5 #) and three groups of THF holes (3 # hole of group 23, 4 # hole of group 24, and 4 # hole of group 30) during a 2 month period.

$$S_{pv} = \frac{(q_1 + q_3 - q_2 - q_4)(t_3 - t_1)}{2} \tag{12}$$

where q_1, q_2, q_3, and q_4 are different pure volumes at various days.

From the actual values, the difference in drainage pure volume between PHF and THF was 6091.2 m^3.

Fig. 12 shows the production histogram and cumulative production of the reservoir by PHF and THF. By comparison, the production per month of PHF was greater than that of THF; moreover, the production of the fourth month by PHF reached the maximum values, longer than that by THF. The cumulative production by PHF per year was 5.29×10^5 m^3, with a mean data production of 1450 m^3/d, while that by THF was 4.08×10^5 m^3, with a mean data production of 1120 m^3/d. These results all showed that PHF had greater fracturing capacity than THF by weakening the reservoir strength and forming complicated fracture networks.

5.3. Change of permeability

Coal is a porous medium and has a natural ability to absorb CBM.

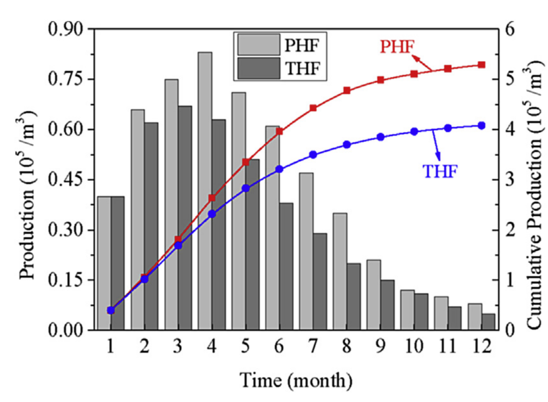

Fig. 12. Production histogram and cumulative production of reservoir by PHF and THF.

In general, the surface area of the coal determines the quantity of coal-surface adsorbed gas, and the size of the coal surface area is related to the pore characteristics of the coal (Busch et al., 2003;

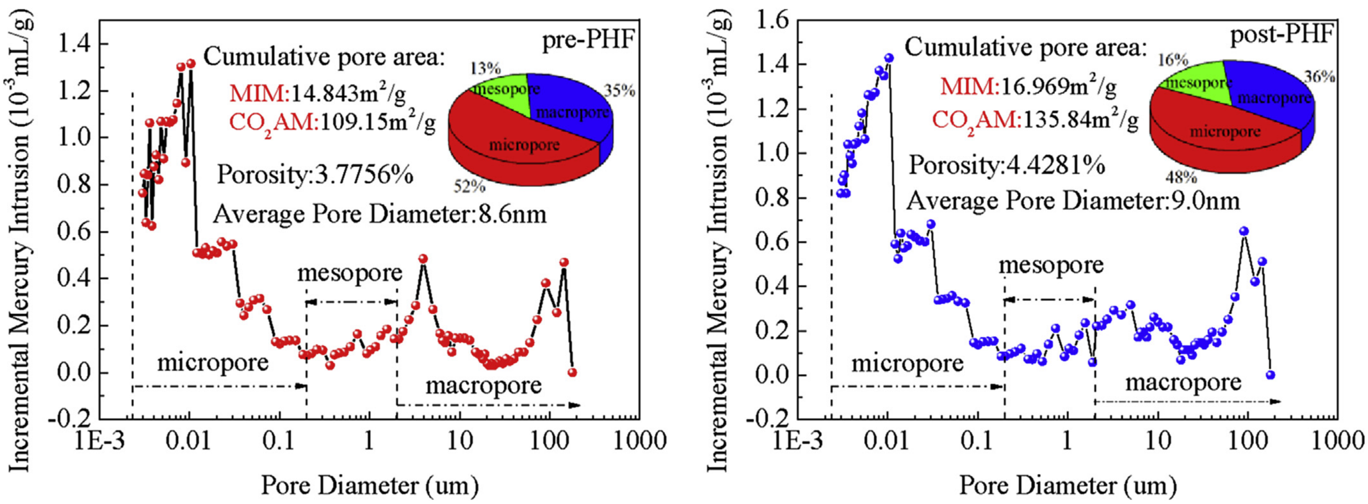

Fig. 13. Incremental mercury intrusion variation at different pore diameters measured by MIM of cores for pre-PHF and post-PHF samples and related parameters measured using MIN and CO_2AM.

Clavaud et al., 2008; Dutta et al., 2011; Weniger et al., 2012; Pan et al., 2012). Therefore, evaluation of pore characteristics of coal is significant to assess the changes of permeability to compare the pre-PHF and post-PHF conditions. Currently, commonly used test methods for pore characteristics are mercury intrusion experiments, nuclear magnetic resonance, and gas adsorption (Gawor and Skoczylas, 2014; Ni et al., 2015; Zou et al., 2014a,b, Liu et al., 2015). The mercury intrusion method (MIM) and the CO_2 adsorption method (CO_2AM) were synthetically used to measure the changes in pore size to assess the permeability changes in this study. We drilled some cores both prior to and after PHF at same distance from the fracturing hole, and measured the pore parameters using MIM and CO_2AM.

From Fig. 13, the incremental mercury intrusion of the smaller-scale micropores increased, indicating that PHF relatively enlarged the scale of the micropores, whereas the changes in mesopores and macropores showed local variation. The fatigue damage resulting from PHF persistently loaded the cores and shocked the grains around all three types of pores under the effect of the exciting oscillation, and thus malpositioning, slippage, and fracturing of pores occurred, which resulted in changes in the primary size and shape of pores. The proportion of micropores, mesopores, and macropores decreased by 7.7% and increased by 23.1% and 2.9%, respectively, relative to the pre-PHF condition. Changes in the pore size induced variation of superficial area, and desorption of CBM might have led to deformation of pores, which influenced the mercury intrusion. Under the effect of crustal stress, compaction and collapse occurred in macropores, most of the macropores became mesopores, so the increase was largest for mesopores. For pre-PHF samples, the cumulative pore areas measured by MIM and CO_2AM were 14.843 and 109.15 m^2/g, respectively, whereas the post-PHF values were 16.969 and 135.84 m^2/g, respectively. The cumulative pore areas increased by 2.126 m^2/g and 26.69 m^2/g for MIM and CO2AM, respectively. The pre-PHF and post-PHF porosity values were 3.7756% and 4.4281%; thus, this field application of PHF with crossing holes had a significant effect in improving the permeability of CBM reservoirs.

6. Conclusions

The primary conclusions of this paper are as follows:

(1) Pulse pressure water flowed in the fractures and propagated pulse waves into internal rocks, inducing cumulative fatigue damage by exciting oscillation and finally decreasing the fracturing strength. When pulse water encountered a non-penetrated crack, eddies were generated, which increased the pressure amplitude under the reflex action of the crack plane. This coupled mechanism is characteristic of PHF and has a stronger effect than THF.

(2) PFC^{2D} was used to compare the difference between PHF and THF for different values of the side-pressure ratio *k*. The results showed that fracturing paths conformed to the law that cracks always form along the direction perpendicular to the minimum principal stress. The fracturing pressure for PHF was lower than that for THF. Furthermore, the number of cracks produced by PHF was greater than that by THF.

(3) A mechanical model for an expanding packer under fracture water pressure loads was estimated based on the upper crossing fracturing hole, and the pressure of the packer was calculated. After PHF, there exists positive correlation between duration and water volume (fitting coefficient 0.9643), as well as fracturing radius (fitting coefficient 0.966), i.e., the longer the duration, the greater the water volume and the greater the fracturing radius. The parameters, included duration and water volume. All the fracturing pressure values for five fracturing holes were smaller than the initiation fracture pressure for THF.

(4) During the process of extraction during the 60 days after PHF, the drainage parameters displayed approximately similar variation. Three phases could be identified based on changes in these parameters: water blocking, rising, and attenuation. Area quantification analysis based on a two-dimensional area was used to compare the difference between PHF and THF. The difference in the drainage pure volume was 6091.2 m^3, demonstrating that the fracturing effect from PHF was better than that from THF.

(5) The field application showed that the proportion of micropores decreased by 7.7%, while the proportion of mesopores and macropores increased by 23.1% and 2.9% after PHF, respectively, which represented a significant improvement in the permeability of the CBM reservoirs.

Acknowledgements

This work was financially supported by the Fundamental Research Funds for the Central Universities (2014XT02),and the Program for Changjiang Scholars and Innovative Research Team in University(IRT13098).

References

Busch, A., Krooss, B.M., Gensterblum, Y., Bergen, F., Pagnier, H.J.M., 2003. High-pressure adsorption of methane, carbon dioxideand their mixtures on coals with a special focus on the preferential sorption behaviour. J. Geochem. Explor 78–79, 671–674.

Cai, Y.D., Liu, D.M., Yao, Y.B., Li, J.Q., Qiu, Y.K., 2011. Geological controls on prediction of coalbed methane of No. 3 coal seam in Southern Qinshui Basin, North China. Int. J. Coal Geol. 88, 101–112.

Chen, L.C., Wang, S.W., He, J.H., Zhang, X.F., Hu, Q., Zhang, Y.C., 2016. CBM reservoir heterogeneity and its controlling effect on gas wells productivity. J. China Univ. Min. Technol. 45, 105–110.

Cheng, Y.P., Wang, L., Zhao, X.L., 2011. Environmental impact of coal mine methane emissions and responding strategies in China. Int. J. Greenh. Gas. Con. 5, 157–166.

Cheng, W., Jin, Y., Chen, M., 2015. Reactivation mechanism of natural fractures by hydraulic fracturing in naturally fractured shale reservoirs. J. Nat. Gas. Sci. Eng. 23, 431–439.

Cho, N., Martin, C.D., Sego, D.C., 2007. A clumped particle model for rock. Int. J. Rock Mech. Min. 44, 997–1010.

Clavaud, J., Maineult, A., Zamora, M., Rasolofosaon, P., Schlitter, C., 2008. Permeability anisotropy and its relations with porous medium structure. J. Geophys. Res. http://dx.doi.org/10.1029/2007JB005004.

Dehkhoda, S., Hood, M., 2013. An experimental study of surface and sub-surface damage in pulsed water-jet breakage of rocks. Int. J. Rock Mech. Min. 63, 138–147.

Dutta, P., Bhowmik, S., Das, S., 2011. Methane and carbon dioxide sorption on a set of coals from India. Int. J. Coal Geol. 85, 289–299.

Ferrer, I., Thurman, E.M., 2015. Chemical constituents and analytical approaches for hydraulic fracturing waters. Trends Environ. Anal. Chem. 5, 18–25.

Fiorotto, V., Rinaldo, A., 1992. Fluctuating uplift and lining design in spillway stilling basins. J. Hydr. Eng. 118, 578–596.

Gawor, M., Skoczylas, N., 2014. Sorption rate of carbon dioxide on coal. Transp. Porous Med. 101, 269–279.

Hu, D., Wang, X.C., Kang, Y., Wang, Z.F., 2016. Oscillating characteristics of the self-excited pulsed air-water jet and its erosion performance of coal-rock. J. China Univ. Min. Technol. 44, 983–989.

Huang, B.X., Liu, C.Y., Fu, J.H., Guan, H., 2011. Hydraulic fracturing after water pressure control blasting for increased fracturing. Int. J. Rock Mech. Min. 48, 976–983.

Huang, W.Y., Yan, S.L., Liu, Z.G., 2012. Research and application of coal mine gas extraction water gel column in the deep hole blasting of coal seam. Int. J. Min. Sci. Tech. 37, 472–476.

Huang, B.X., Li, P.F., Ma, J., Chen, S.L., 2014a. Experimental investigation on the basic law of hydraulic fracturing after water pressure control blasting. Rock Mech. Rock Eng. 47, 1321–1334.

Huang, Z., Jiang, Z.Q., Zhu, S.Y., Qian, Z.W., Cao, D.T., 2014b. Characterizing the hydraulic conductivity of rock formations between deep coal and aquifers using injection tests. Int. J. Rock Mech. Min. 71, 12–18.

Hubbert, M.K., Willis, D.G., 1957. Mechanics of hydraulic fracturing. Am. Soc. Min. Eng. 210, 153–168.

Jin, K., Cheng, Y.P., Wang, L., Dong, J., Guo, P.K., An, F.H., Jiang, L.M., 2015. The effect of sedimentary redbeds on coalbed methane occurrence in the Xutuan and Zhaoji Coal Mines, Huaibei Coalfield, China. Int. J. Coal Geol. 137, 111–123.

Kang, H.P., Feng, Y.J., 2012. Monitoring of stress change in coal seam caused by directional hydraulic fracturing in working face with strong roof and its evolution. J. China Coal Soc. 37, 1953–1959.

Li, X.Z., 2013. The Mechanism and Technology of Permeability Enhancements in Coal Seam Based on High Pressure Pulsating Hydraulic Fracturing. Dissertation. China University of Mining and Technology.

Li, A.H., Liu, P.Q., 2005. Models for simulating the propagation of fluctuating pressure in gaps of stilling basin slab. J. Hydr. Eng. 36, 1236–1240.

Li, Q.G., Zhai, C., Lin, B.Q., Li, X.Z., 2011. The Method of Gas Extraction by Pulse Fracturing Antireflection in Low Permeability Coal Seam. Patent (in Chinese).

Li, X.Z., Lin, B.Q., Zhai, C., Li, Q.G., Ni, G.H., 2013. The mechanism of breaking coal and rock by pulsating pressure wave in single low permeability seam. J. Ch., Coal Soc. 38, 918–923.

Li, Q.G., Lin, B.Q., Zhai, C., Ni, G.H., Li, X.Z., Sun, C., 2013a. Experimental study on action characteristic of pulsating parameters in coal seam pulse hydraulic fracturing. J. Ch. Coal Soc. 38, 1185–1190.

Li, Q.G., Lin, B.Q., Zhai, C., Ni, G.H., Peng, S., Sun, C., Cheng, Y.Y., 2013b. Variable frequency of pulse hydraulic fracturing for improving permeability in coal seam. Int. J. Min. Sci. Tech. 23, 847–853.

Li, Q.G., Lin, B.Q., Zhai, C., 2015. A new technique for preventing and controlling coal and gas outburst hazard with pulse hydraulic fracturing: a case study in Yuwu coal mine, China. Nat. Hazards 75, 2931–2946.

Li, H., Lin, B.Q., Yang, W., Zheng, C.S., Hong, Y.D., Gao, Y.B., Liu, T., Wu, S.L., 2016. Experimental study on the petrophysical variation of different rank coals with microwave treatment. Int. J. Coal. Geol. 154–155, 82–91.

Liang, W.G., Zhang, C.D., Gao, H.B., Yang, X.Q., Xu, S.G., Zhao, Y.S., 2012. Experiments on mechanical properties of salt rocks under cyclic loading. J. Rock Mech. Geotech. Eng. 4, 54–61.

Liu, P.Q., 1994. Study of the Mechanism of Scour by Free Jets on Rocky River Beds. Dissertation. Tsinghua University.

Liu, P.Q., Deng, X.Y., 1998. Numerical investigation of pressure fluctuations within crack layers of lower surfaces of slabs. Acta. Mech. Sin. 30, 662–671.

Liu, E.L., He, S.M., 2012. Effects of cyclic dynamic loading on the mechanical properties of intact rock samples under confining pressure conditions. Eng. Geol. 125, 81–91.

Liu, J.S., Chen, Z.W., Elsworth, D., Qu, H.Y., Chen, D., 2011. Interactions of multiple processes during CBM extraction: a critical review. Int. J. Coal Geol. 87, 175–189.

Liu, C.J., Wang, G.X., Sang, S.X., Gilani, W., Rudolph, V., 2015. Fractal analysis in pore structure of coal under conditions of CO_2 sequestration process. Fuel 139, 125–132.

Lu, P., Li, G.S., Huang, Z.W., Tian, S.C., Shen, Z.H., 2014. Simulation and analysis of coal seam conditions on the stress disturbance effects of pulsating hydro-fracturing. J. Nat. Gas. Sci. Eng. 21, 649–658.

Lu, P.Q., Li, G.S., Huang, Z.W., He, Z.G., Li, X.J., Zhang, H.Y., 2015. Modeling and parameters analysis on a pulsating hydro-fracturing stress disturbance in a coal seam. J. Nat. Gas. Sci. Eng. 26, 253–263.

Nakao, S., Najita, J., Karasaki, K., 2000. Hydraulic well testing inversion for modeling fluid flow in fractured rocks using simulated annealing: a case study at Raymond field site, California. J. Appl. Geophys. 45, 203–223.

Ni, G.H., Lin, B.Q., Zhai, C., Li, Q.G., Peng, S., Li, X.Z., 2014. Kinetic characteristics of coal gas desorption based on the pulsating injection. Int. J. Min. Sci. Tech. 24, 631–636.

Ni, X.M., Li, Q.Z., Wang, Y.B., Gao, S.S., 2015. Permeability variation characteristics of coal after injecting carbon dioxide into a coal seam. Int. J. Min. Sci. Tech. 25, 665–670.

Ni, G.H., Cheng, W.M., Lin, B.Q., Zhai, C., 2016. Experimental study on removing water blocking effect (WBE) from two aspects of the pore negative pressure and surfactants. J. Nat. Gas. Sci. Eng. 31, 596–602.

Palmer, I., 2010. Coalbed methane completions: a world view. Int. J. Coal. Geol. 82, 184–195.

Pan, J.N., Hou, Q.L., Ju, Y.W., Bai, H.L., Zhao, Y.Q., 2012. Coalbed methane sorption related to coal deformation structures at different temperatures and pressures. Fuel 102, 760–765.

Potyondy, D.O., Cundall, P.A., 2004. A bonded-particle model for rock. Int. J. Rock Mech. Min. 41, 1329–1364.

Sang, S.X., Xu, H.J., Fang, L.C., Li, G.J., Huang, H.Z., 2010. Stress relief coalbed methane drainage by surface vertical wells in China. Int. J. Coal Geol. 82, 196–203.

Sesetty, V., Ghassemi, A., 2015. A numerical study of sequential and simultaneous hydraulic fracturing in single and multi-lateral horizontal wells. J. Pet.. Sci. Eng. 132, 65–76.

Shimizu, H., Murata, S., Ishida, T., 2011. The distinct element analysis for hydraulic fracturing in hard rock considering fluid viscosity and particle size distribution. Int. J. Rock Mech. Min. 48, 712–727.

Su, X.B., Lin, X.Y., Liu, S.B., Zhao, M.J., Song, Y., 2005. Geology of coalbed methane reservoirs in the southeast Qinshui basin of China. Int. J. Coal Geol. 62, 197–210.

Vedachalam, N., Srinivasalu, S., Rajendran, G., Ramadass, G.A., Atmanand, M.A., 2015. Review of unconventional hydrocarbon resources in major energy consuming countries and efforts in realizing natural gas hydrates as a future source of energy. J. Nat. Gas. Sci. Eng. 26, 163–175.

Vijay, M.M., Remisz, J., Shen, X., 1993. Potential of pulsed water jets for cutting and fracturing of hard rock formations. Int. J. Surf. Min. Recl. Environ. 7, 121–132.

Wang, H.F., Cheng, Y.P., Wang, W., Xu, R., 2014a. Research on comprehensive CBM extraction technology and its applications in China's coal mines. J. Nat. Gas. Sci. Eng. 20, 200–207.

Wang, T., Zhou, W.B., Chen, J.H., 2014b. Simulation of hydraulic fracturing using particle flow method and application in a coal mine. Int. J. Coal Geol. 121, 1–13.

Wang, W.C., Li, X.Z., Lin, B.Q., Zhai, C., 2015. Pulsating hydraulic fracturing technology in low permeability coal seams. Int. J. Min. Sci. Tech. 25, 681–685.

Weniger, P., Franců, J., Hemza, P., Krooss, B.M., 2012. Investigations on the methane and carbon dioxide sorption capacity of coals from the SW Upper Silesian Coal Basin, Czech Republic. Int. J. Coal. Geol. 93, 23–39.

Xie, H.P., Ju, Y., Dong, L.L., 1997. Discussion of elastic modulus method defined in classic damage. Mech. Eng. 19, 1–5.

Yoon, J.S., Zimmermann, G., Zang, A., 2015. Numerical investigation on stress shadowing in fluid injection-induced fracture propagation in naturally fractured geothermal reservoirs. Rock Mech. Rock Eng. 48, 1439–1454.

Zhai, C., Li, X.Z., Li, Q.G., 2011. Research and application of coal seam pulse hydraulic fracturing technology. J. Ch. Coal. Soc. 36, 1996–2001.

Zhai, C., Li, M., Sun, C., Zhang, J.G., Yang, W., Li, Q.G., 2012. Guiding-controlling technology of coal seam hydraulic fracturing fractures extension. Int. J. Min. Sci. Tech. 22, 831–836.

Zhai, C., Yu, X., Xiang, X.W., Li, Q.G., Wu, S.L., Xu, J.Z., 2015a. Experimental study of pulsating water pressure propagation in CBM reservoirs during pulse hydraulic fracturing. J. Nat. Gas. Sci. Eng. 25, 15–22.

Zhai, C., Xu, J.Z., Xiang, X.W., Zhong, C., 2015b. Flexible gel (FG) for gas-drainage drilling sealing material based on orthogonal design. Int. J. Min. Sci. Tech. 25,

1031–1036.
Zhang, J.C., 2014. Numerical simulation of hydraulic fracturing coalbed methane reservoir. Fuel 136, 57–61.
Zhao, Z.B., 2008. Study of technology of variable-frequency pulse water infusion into coal seam. J. Min. Saf. Eng. 25, 486–489.
Zhao, Q., Lisjak, A., Mahabadi, O., Liu, Q.Y., Grasselli, G., 2014. Numerical simulation of hydraulic fracturing and associated microseismicity using finite-discrete element method. J. Rock Mech. Geotechn. Engin 6, 574–581.
Zhou, J., Jin, Y., Chen, M., 2010. Experimental investigation of hydraulic fracturing in random naturally fractured blocks. Int. J. Rock Mech. Min. 47, 1193–1199.
Zhou, L., Hou, M.Z., Gou, Y., Li, M.T., 2014. Numerical investigation of a low-efficient hydraulic fracturing operation in a tight gas reservoir in the North German Basin. J. Pet.. Sci. Engin 120, 119–129.
Zhu, H.Q., Zhang, M.B., Shen, J., Hu, R.L., 2013. Permeability enhancing mechanism and numerical analysis on pulsating water injection in low permeability coal seams. J. China. Coal. Soc. 38, 343–347.
Zhu, H.Q., Zhang, M.B., Gu, B.F., Shen, X., Zhu, S.H., 2014. Experimental analysis of damage deformation of low permeability and soft coal under pulsating water pressure. J. Ch. Coal Soc. 39, 1269–1274.
Zou, Q.L., Lin, B.Q., Liu, T., Zhou, Y., Zhang, Z., Yan, F.Z., 2014a. Variation of methane adsorption property of coal after the treatment of hydraulic slotting and methane pre-drainage: a case study. J. Nat. Gas. Sci. Eng. 20, 396–406.
Zou, Q.L., Lin, B.Q., Liang, J.Y., 2014b. Variation in the pore structure of coal after hydraulic slotting and gas drainage. Adsorpt. Sci. Tech. 32, 647–666.